ARTICLES

Intramolecular Electron and Energy Transfer in an Axial ZnP−Pyridylfullerene Complex As Studied by X- and W-Band Time-Resolved EPR Spectroscopy

Tamar Galili,[†] Ayelet Regev,[†] Alexander Berg,[†] Haim Levanon,*[,†,⊥] David I. Schuster,*[,‡,∥] Klaus Möbius,[§] and Anton Savitsky[§]

Department of Physical Chemistry and the Farkas Center for Light-Induced Processes, The Hebrew University of Jerusalem, Jerusalem 91904, Israel, Department of Chemistry, New York University, New York, New York 10003, and Institut für Experimentalphysik, Freie Universität Berlin, Arnimallee 14, D-14195 Berlin, Germany

Received: May 31, 2005; In Final Form: August 8, 2005

Light-driven electron transfer (ET) and energy transfer (EnT) in a self-assembled via axial coordination Zn−porphyrin−pyridylfullerene (ZnP−PyrF) complex were studied by time-resolved electron paramagnetic resonance (TREPR) spectroscopy at 9.5 GHz (X-band) and 95 GHz (W-band). The studies over a wide temperature range were carried out in media of different polarity, including isotropic toluene and tetrahydrofuran (THF), and anisotropic nematic liquid crystals (LCs), E-7 and ZLI-4389. At low temperatures (frozen matrices), photoexcitation of the ZnP donor results mainly in singlet−singlet EnT to the pyridine-appended fullerene acceptor. In fluid phases ET is the dominant process. Specifically, in isotropic solvents the generated radical pairs (RPs) are long-lived, with lifetimes exceeding that observed for covalently linked donor−acceptor systems. It is concluded that in liquid phases of both polar and nonpolar solvents the separation of the tightly bound complex into the more loosely bound structure slows down the back ET (BET) process. Photoexcitation of the donor in fluid phases of LCs does not result in the creation of the long-lived RPs, since the ordered LC matrix hinders the separation of the complex constituents. As a result, fast intramolecular BET takes place in the tightly bound complex. Contrarily to the behavior of covalently linked donor−acceptor systems in different LCs, the polarity of the LC matrix affects the ET process. Moreover, in contrast to covalently linked D−s−A systems, utilization of LCs for the coordinatively linked D−s−A complexes does not reduce the ET rates significantly.

Introduction

Efficient conversion of solar into chemical energy in natural photosynthetic system has inspired modern photochemistry research for many years. Among biomimetic systems,[1−3] porphyrin−fullerene complexes are most attractive as electron donor−acceptor (D−A) systems, due to the celebrated electron donor properties of porphyrins (D) and the unique electron-accepting properties of fullerenes (A).[4−6] An important requirement for an effective electron transfer (ET) process is to minimize undesirable energy-wasting reactions such as charge recombination and energy transfer (EnT) from the donor to the acceptor, processes that may compete with efficient charge separation. Increasing the solvent polarity results in stabilization of the charge-separated state, thus favoring ET over EnT. To overcome fast back electron transfer (BET), which characterizes many covalently linked D−A systems, employment of systems linked via hydrogen bonds, van der Waals forces, electrostatic interactions, $\pi-\pi$ stacking, or metal−ligand coordination has attracted attention.[7−10] In such noncovalent systems, the fast and efficient charge separation takes place within their intramolecular configuration generated via molecular recognition. In the case of metal−ligand complexation, dissociation of the charge-separated state may occur, in the limit turning charge recombination into an intermolecular process. With respect to porphyrin−fullerene D−A systems, the utilization of fullerene derivatives with an attached pyridine spacer enables complexation with the kinetically labile metal center of zinc porphyrin.[7,9,11−17] Association by such an interaction is reversible, as equilibrium between bound and unbound states is established. The complex dissociation rate depends on the strength of the coordination bond, thus permitting stabilization of the charge separated states.

We report here on a time-resolved electron paramagnetic resonance (TREPR) study of a pyridinofullerene (PyrF) ligand forming a D−s−A complex (Scheme 1) with zinc tetraphenylporphyrin (ZnP), where ZnP is the donor (D) and PyrF is the acceptor attached to the spacer (s−A). We employed

* Corresponding authors.
[†] The Hebrew University of Jerusalem.
[‡] New York University.
[§] Freie Universität Berlin.
[⊥] Telephone: +972-2-658-5544. Fax: +972-2-651-8383. E-mail: levanon@chem.ch.huji.ac.il.
[∥] Telephone: +1-212-998-8447. Fax: +1-212-260-7905. E-mail: david.schuster@nyu.edu.

10.1021/jp052873r CCC: $30.25
Published on Web 09/07/2005

SCHEME 1

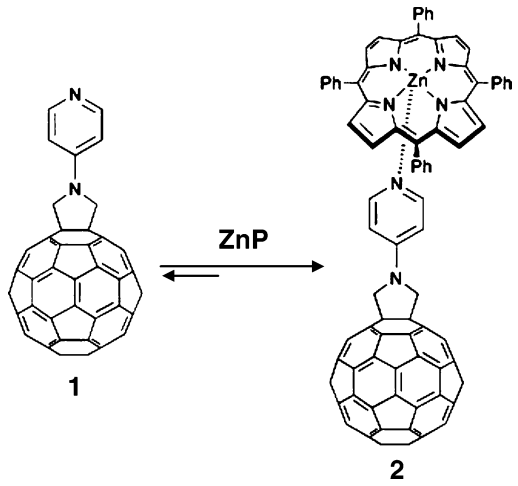

TREPR both at X-band (9.5 GHz) and W-band (95 GHz) to utilize the corresponding increase of the external magnetic field to discriminate between field-dependent and field-independent spin polarization mechanisms in photoinduced ET and EnT processes. This enabled us to unambiguously characterize the RP formation.

Preliminary optical studies on ZnP−PyrF complex made at room temperature show that fluorescence quenching of ZnP occurs efficiently in both nonpolar and polar solvents.[18,19] The mechanisms responsible for the fluorescence quenching were not established. The present TREPR study is focused on understanding the role of ET and EnT in this system following photoexcitation. TREPR spectroscopy, coupled with laser photoexcitation, proved to be a useful method in studying paramagnetic transients born in photodriven reactions. Such intermediates can be accurately identified through their magnetic properties. Moreover, the use of anisotropic liquid crystals (LCs), with their unique ordering properties, allows one to follow by TREPR temperature-dependent processes over a wide temperature range.[20−26]

Experimental Section

The schematic structure of Zn−tetraphenylporphyrin−pyridylfullerene complex (ZnP−PyrF) is shown in Scheme 1. Its synthesis and photophysical properties are described elsewhere.[18,19] As described earlier,[27] continuous-wave (CW) X-band (9.5 GHz) TREPR studies of the photoexcited triplet and photoinduced charge separated states of the ZnP−PyrF complex were carried out on a Bruker ESP-380 CW spectrometer with the field modulation disconnected. CW W-band (95 GHz) TREPR studies were carried out on an EPR spectrometer, designed and built in FU Berlin, with a single-mode TE_{011} cylindrical cavity.[28]

The TREPR measurements were performed in different isotropic matrices such as toluene and tetrahydrofuran (THF) (Merck Ltd) and anisotropic nematic liquid crystals (LCs) such as E-7 and ZLI-4389 (Merck Ltd), in which the chromophores could be partially oriented. Toluene was dried over molecular sieves and THF was distilled from sodium and benzophenone solution. The two solvents of each set were chosen due to the difference in their dielectric constants: $\epsilon_{toluene} = 2.38$; $\epsilon_{THF} = 7.58$;[29] $\epsilon_{E-7} = 19.0$; and $\epsilon_{ZLI-4389} = 56.0$.[30] The solutions of ZnP−PyrF complex were prepared by 1:1 mixing of equimolar solutions of ZnP and PyrF in a given solvent (toluene or THF). X-band EPR samples (∼0.5 mM) were prepared in 4 mm o.d. Pyrex tubes and degassed by several freeze−pump−thaw cycles on a vacuum line. LC samples were prepared by first dissolving the both chromophores in toluene, preparation of the 1:1 mixture, introducing of the mixture in to the EPR tubes and then, after evaporation of toluene, introduction of LC. The EPR samples (∼0.5 mM) for W-band experiments were prepared in 0.6 mm i.d. (0.84 o.d.) quartz capillaries, deoxygenated by repeated freeze−pump−Ar saturation−thaw cycles on a vacuum line and sealed under vacuum.

TREPR experiments were carried out over a broad range of temperatures according to the phase diagrams for each solvent:

E-7: crystalline $\xrightarrow{210\ K}$ soft crystalline $\xrightarrow{263\ K}$ nematic $\xrightarrow{333\ K}$ isotropic

ZLI-4389: crystalline $\xrightarrow{250\ K}$ soft crystalline $\xrightarrow{253\ K}$ nematic $\xrightarrow{335\ K}$ isotropic

toluene: glass $\xrightarrow{117\ K}$ amorphous $\xrightarrow{178\ K}$ liquid

THF: glass $\xrightarrow{164.5\ K}$ liquid

Temperature was maintained by using a variable-temperature nitrogen flow Dewar in the X-band EPR resonator and by a stabilized nitrogen gas-flow system in the W-band cryomagnet.

In X-band experiments the samples were photoexcited at 532 nm (∼10 mJ/pulse at a repetition rate of 10 Hz) by an OPO laser (Continuum Panther SLII-10) pumped by a third harmonic of a Nd:YAG laser (Continuum Surelite II-10). The photoexcitation wavelength was chosen according to the absorption spectra of the complex constituents, mainly exciting the ZnP component, since the extinction coefficients at 532 nm are of $\sim 5 \times 10^3\ M^{-1}\ cm^{-1}$ for ZnP[31] and of $\sim 0.9 \times 10^3\ M^{-1}\ cm^{-1}$ for PyrF.[32] In W-band experiments, the samples were excited at 532 nm by the second harmonic of Nd:YAG laser employing a quartz fiber of 0.8 mm diameter.

Two distinct orientations of the samples with respect to the magnetic field, B, were studied in the crystalline phase of the LCs, namely L||B and L⊥B, where L is the LC director. The initial alignment of the sample is L||B, and the L⊥B orientation is obtained by rotating the sample in the microwave cavity by $\pi/2$ about an axis perpendicular to B. In the fluid phases, at higher temperatures (soft crystalline and nematic phases), only the L||B orientation is maintained. At these temperatures, molecular motion is allowed and rotation of the sample results in a fast molecular reorientation, back to the initial parallel configuration.

For comparison, control experiments were carried out on the separate complex constituents (i.e., PyrF and ZnP) and on a 1:1 mixture of ZnP and pristine C_{60} (ZnP:C_{60}).

Results and Discussion

PyrF (**1** in Scheme 1) was designed to provide direct electronic communication between fullerene (C_{60}) and the pyridyl N atom and between C_{60} and ZnP upon complexation (**2** in Scheme 1). The association constant K_a in *ortho*-dichlorobenzene was found to be $7.4 \times 10^4\ M^{-1}$.[18,19] This value corresponds to a bond energy of ∼6−7 kcal M^{-1}. Calculations show that with this association constant ∼85% of the ZnP and PyrF moieties are linked through ligand complexation. The absence of EPR signals of the free species suggests a similar degree of complexation in all solvents used. Electron density calculations made on the axially symmetric complex **2** indicate that effective electronic interaction between ZnP and C_{60} occurs

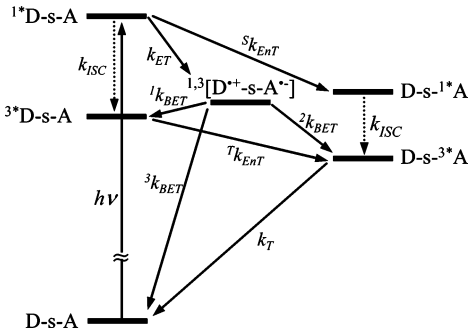

Figure 1. General presentation of the energy level scheme and the relevant processes taking place in a D−s−A system after photoexcitation. The energy levels of D$^{\bullet+}$−s−A$^{\bullet-}$ are chosen arbitrarily for the case where they lie between the ^{3*}D−s−A and D−s−^{1*}A states. All the abbreviations are described in the text.

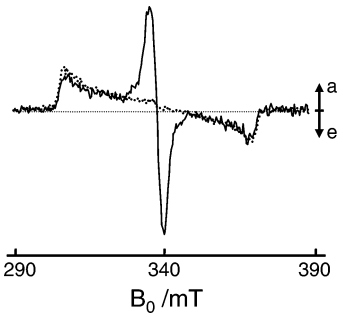

Figure 2. X-band TREPR spectra $\chi''(B_0)$ of photoexcited ZnP:C_{60} 1:1 mixture (dotted), and ZnP−PyrF complex (solid), both taken in toluene at 130 K, 0.8 μs after the laser pulse (positive and negative signals with respect to the baseline indicate absorption (a) and emission (e), respectively).

directly through the two nitrogen atoms.[18,19] According to molecular modeling, the center-to-center distance (R_{cc}) for the axially symmetric complex **2** is 11.99 Å, and the center-to-edge distance, i.e., porphyrin to fullerene (R_{ce}) is 9.34 Å.[18] An X-ray structure shows that in the solid state, the ZnP−PyrF complex is indeed axially symmetric with $R_{cc} = 12.18$ Å and $R_{ce} = 8.56$ Å.[19] However, calculations using molecular dynamics indicate that a bent conformer in which $R_{cc} = 9.21$ Å may also play a role.[18,33]

Photoexcitation of a 1:1 mixture of ZnP and pristine C_{60} resulted in a mixture of ^{3*}ZnP (dominant) and $^{3*}C_{60}$ EPR spectra, in line with the extinction coefficients of the chromophores at 532 nm. In the absence of additional interactions, it is expected that selective excitation of the 1:1 ZnP−PyrF complex should yield results similar to those obtained for a 1:1 mixture of ZnP and pristine C_{60}. However, this is not the case. The experimental results presented below point on efficient communication between the complex constituents, which indicates the ZnP−PyrF complex **2** as a functioning D−s−A system. The sequence and energetics of photoinduced processes in a general D−s−A system are depicted in Figure 1.

Photoexcitation of the donor part of ZnP−PyrF complex brings it to the first excited singlet state, ^{1*}ZnP−PyrF, triggering a series of downhill reactions along an energy gradient. Following this initial step, the charge-separated radical pair (RP) signals are observed over a broad temperatures range indicating an active ET route. Observation of ET at low temperatures confirms the existence of the bound complex, since ET between unbound constituents is diffusion-controlled process and cannot take place in frozen solutions.

As was described in detail elsewhere,[23,34−36] there are two possible mechanisms of intramolecular ET to produce the RP states, i.e., spin correlated radical pair (SCRP) and triplet radical pair (TRP) mechanisms. SCRP is governed by both the spin−spin exchange interaction, ***J***, and by the electron−electron dipolar interaction, ***D***, quantified by the zero-field splitting (ZFS) parameters D and E. In covalently linked systems with sufficiently long D−A distances (∼18−24 Å), where multistep ET takes place, the observed RPs were generated via SCRP mechanism.[23,36] SCRPs were also observed in hydrogen bonded D−A complexes.[37−39] A characteristic feature in the SCRP spectrum are two antiphase doublets, centered at the g-factors of the individual radicals, while ***J*** and ***D*** determine the splitting in each doublet. The separation of the two doublets is field dependent and proportional to $\Delta g\beta B_0$, where Δg is the difference in g-factors of the radicals, β is the Bohr magneton, and B_0 is the external magnetic field.

The TRP mechanism is governed by dipolar interaction only. Such a mechanism is operative in systems with $J \gg D$ as was observed in covalently linked systems with short D−A distances which undergo single-step ET.[23,24,26,40] The TRP spectrum is centered about the mean value of the g-factors of the RP's constituents, where the ZFS parameter D determines the spectral width. It is clear that the TRP spectrum should have the same width at X- and W-band frequencies, while the SCRP spectrum has different widths due to its dependence on $\Delta g\beta B_0$. Comparison of X- and W-band results should shed light on the nature of the observed RPs. In addition, for each mechanism, the polarization pattern of the RP spectrum explicitly reveals its precursor, i.e., the singlet or triplet excited state of the donor. Furthermore, a phase inversion of the time-evolved RP spectra usually indicates the participation of two ET routes, where singlet-initiated RPs may be accompanied by triplet-initiated RPs.

Isotropic Matrices. ***Toluene.*** TREPR experiments on ZnP−PyrF, dissolved in toluene, were performed in the temperature range of 130−300 K. In frozen toluene (130−178 K), the spectra consist of both ZnP and PyrF triplets within the complex, i.e., ^{3*}ZnP−PyrF and ZnP−^{3*}PyrF. However, the ratio of the two components is smaller than that obtained for the control 1:1 mixture ZnP:C_{60}, indicating a stronger contribution of the fullerene moiety in the ZnP−PyrF complex (Figure 2).

In terms of Figure 1, the enhanced yield of the ZnP−^{3*}PyrF may be due to several routes: (1) singlet−singlet EnT ^{1*}ZnP−PyrF → ZnP−^{1*}PyrF ($^{S}k_{EnT}$), followed by intersystem crossing (ISC) within the PyrF moiety (k_{ISC}); (2) triplet−triplet EnT ^{3*}ZnP−PyrF → ZnP−^{3*}PyrF ($^{T}k_{EnT}$); and (3) BET from the RP state, either directly ZnP$^{\bullet+}$−PyrF$^{\bullet-}$ → ZnP−^{3*}PyrF ($^{2}k_{BET}$) or indirectly ZnP$^{\bullet+}$−PyrF$^{\bullet-}$ → ^{3*}ZnP−PyrF ($^{1}k_{BET}$), followed by ^{3*}ZnP−PyrF → ZnP−^{3*}PyrF ($^{T}k_{EnT}$). All these routes are energetically allowed considering the fact that ^{1*}ZnP is higher than $^{1*}C_{60}$, i.e., 2.12 and 1.80 eV, respectively, and ^{3*}ZnP is higher than $^{3*}C_{60}$, i.e., 1.59 and 1.57 eV, respectively.[41,42] The values for C_{60} are upper limits, since the energy levels of the first excited singlet and triplet states of pyridyl-substituted derivatives are slightly lower (∼0.04−0.10 eV) than those of pristine C_{60}.[43−46] The most probable route was derived by triplet line shape analysis comparing ZnP−^{3*}PyrF to the monomer ^{3*}PyrF. This analysis suggests a singlet−singlet EnT process ($^{S}k_{EnT}$) as the main reason for the enhanced yield of ZnP−^{3*}PyrF.

In frozen toluene (130−178 K), in the time window 3.0−3.5 μs, where the spectral features attributed to ^{3*}ZnP−PyrF and ZnP−^{3*}PyrF completely disappear, a residual weak signal is observed at $g \sim 2$. This signal with peak-to-peak width ΔH_{p-p}

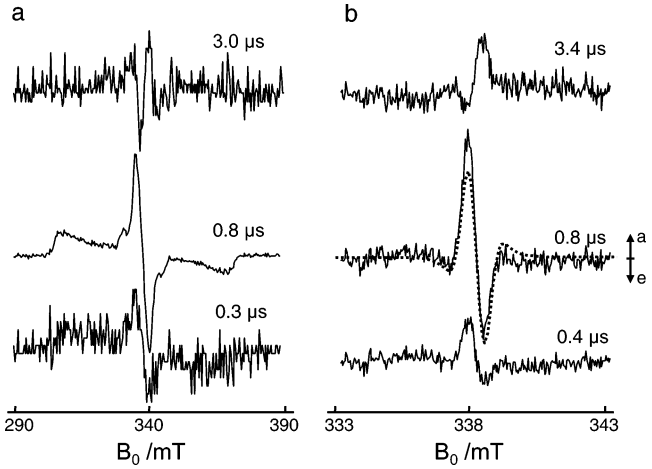

Figure 3. X-band TREPR spectra $\chi''(B_0)$ of photoexcited ZnP−PyrF, taken in toluene at different times after the laser pulse: (a) at 170 K, the spectrum at 0.8 μs was unchanged, while these at 0.3 μs and 3.0 μs were enlarged by a factor of 8; (b) at 200 K, the superimposed dotted line (at 0.8 μs) is the line shape simulation.

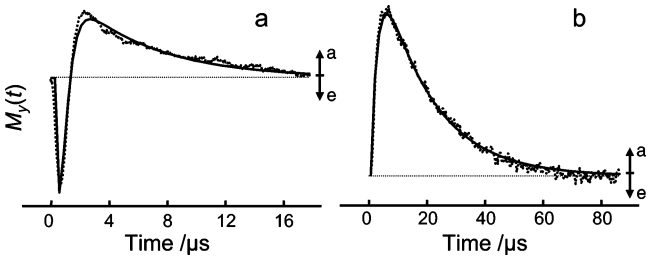

Figure 4. Kinetic profile of the RP ($ZnP^{\bullet+}-PyrF^{\bullet-}$): (a) in liquid toluene at 200 K, taken from the EPR line at 338.3 mT; (b) in liquid THF at 180 K, taken from the EPR line at 337.4 mT. Superimposed solid lines are the best fits to the corresponding experimental curves. The detected EPR signal $\chi''(B_0)$ is proportional to magnetization value M_y.

$\approx$ 3.3 mT, exhibits an **e**, **a** (emission, absorption) polarization pattern, from low to high field, respectively (Figure 3a). It is reasonable to assume that this signal is present also at earlier times, but is masked under the stronger $ZnP-{}^{3*}PyrF$ signal. Within the dipole−dipole approximation, $\Delta H_{p-p} \approx |D| \cong (3/4) \times [(g\beta)^2/r^3]$, the distance between the correlated spins is ~9.3 Å. This value is smaller than R_{cc}, as determined by X-ray analysis. However, a poor signal-to-noise (S/N) ratio of this residual spectrum makes the experimental estimation of R_{cc} somewhat ambiguous. We attribute this signal to the radical ion pair, $ZnP^{\bullet+}-PyrF^{\bullet-}$, which arises on excitation of the tightly bound complex.

In liquid toluene, at 200 K, the spectra of $^{3*}ZnP-PyrF$ and $ZnP-{}^{3*}PyrF$ could not be detected, most likely due to a short spin−lattice relaxation time, leaving only a narrow spectrum at $g \sim 2$. This spectrum displays an **a**, **e** polarization pattern up to ~1.4 μs, evolving in later times into an **e**, **a** signal (Figure 3b).

The spectral behavior, shown in Figure 3b, is also reflected by the temporal changes of the magnetization, $M_y(t)$ after laser excitation at time $t = 0$ (Figure 4a, Figure 4b will be discussed later).

The kinetic profile of the magnetization, $M_y(t)$, of the RP, shown in Figure 4a, was fit with the following fitting function:

$$M_y(t) = A_1 e^{-t/\tau_1} + A_2 e^{-t/\tau_2} + A_3 e^{-t/\tau_3} \qquad (1)$$

where τ_i ($i = 1-3$) are the corresponding rise and/or decay times, and A_i ($i = 1-3$) are the relevant amplitudes of the magnetization, $M_y(t)$. The best fit results are summarized in Table 1. It should be noted that the response time of our TREPR system is ~0.2 μs limits the detection to triplet RPs characterized with rise times on the order of 0.2−0.3 μs. However, the rise time of 0.3 μs obtained for $ZnP^{\bullet+}-PyrF^{\bullet-}$ in toluene, associated with the buildup of the triplet RP, is in line with the ET rate of 2×10^6 s^{-1} observed by TREPR of a similar complex at low temperature.[12]

TABLE 1: Kinetic Data of the Magnetization, $M_y(t)$, of the RPs in Fluid Phases of Different Solvents Derived from Eq 1

medium	T (K)	$\tau_1{}^a$	$\tau_2{}^a$	$\tau_3{}^a$
toluene	200	0.3	0.4	5.6
THF	180	2.4	17.8	
E-7	280	0.3	0.5	0.9

[a] For the triexponential kinetics, τ_1 is the rise time of the singlet-initiated RP, τ_2 is the rise time of the competing triplet-initiated RP, and τ_3 is the decay time of the RP. For the biexponential kinetics, τ_1 is the rise time of the singlet-initiated RP, and τ_2 is the decay time of the RP. All times are in μs.

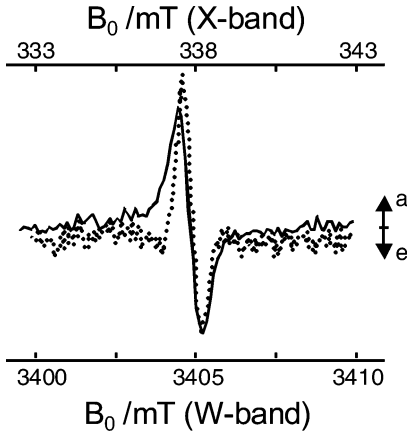

Figure 5. X-band (dotted) and W-band (solid) TREPR spectra $\chi''(B_0)$ of RP ($ZnP^{\bullet+}-PyrF^{\bullet-}$) in toluene at 200 K.

Inspection of Figures 3b and 4a shows that the spectrum reaches its maximum intensity at ~0.8 μs after the laser pulse, with polarization pattern **e**, **a**, **e**, **a**. This spectrum is attributed to the TRP, formed by an $S-T_0$ mixing mechanism (i.e., a singlet precursor), with $D = -0.7$ mT, and $E = 0.1$ mT (uncertainty is ±5% and ±20%, respectively). At later times, the spectrum changes its phase pattern to **e**, **a**. The opposite phase pattern is rationalized in terms of TRP, formed via triplet precursor, where the T_{+1} and T_{-1} levels are populated. High-field EPR experiments at W-band were carried out to confirm that, indeed, the TRP mechanism is responsible for RP generation. As indicated above, the operating mechanism may be revealed by comparing the EPR results at two microwave frequencies. In Figure 5, the RP spectra taken at X- and W-band frequencies are displayed. The isotropic g-factors of $ZnP^{\bullet+}$ and $C_{60}{}^{\bullet-}$ are 2.0025[47] and 1.9999,[48] respectively. Correspondingly, at X-band such Δg would result in a SCRP spectrum with a line separation of 0.455 mT, while at W-band it would correspond to a line separation of 4.55 mT. Comparison of the X- and the W-band spectra, taken in toluene at 200 K, shows that the width of the RP spectrum is the same at both frequencies. This confirms our conclusion that the observed RP is a TRP, i.e., $^3(ZnP^{\bullet+}-PyrF^{\bullet-})$.

With this D value (−0.7 mT) the distance between the interacting spins may be evaluated in dipole−dipole approximation to be ~15.7 Å. This distance (R_{cc}) is larger than that determined by X-ray diffraction for a tightly bound ZnP−PyrF

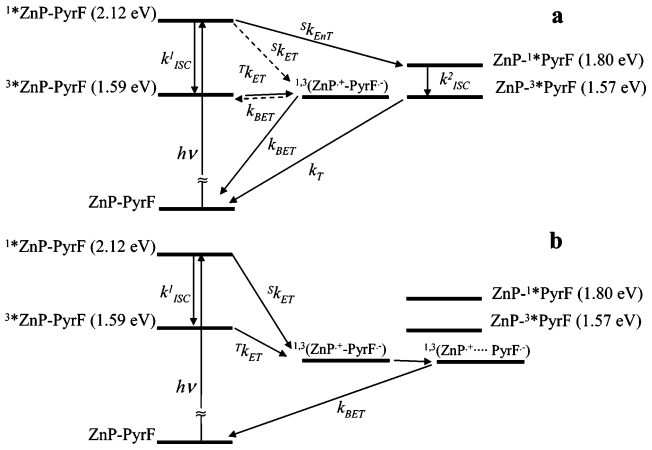

Figure 6. Energy level diagram (unscaled) of ZnP−PyrF in (a) frozen and (b) liquid toluene. The suggested partial dissociation is indicated as $^{1,3}(ZnP^{\bullet+}\cdots PyrF^{\bullet-})$.

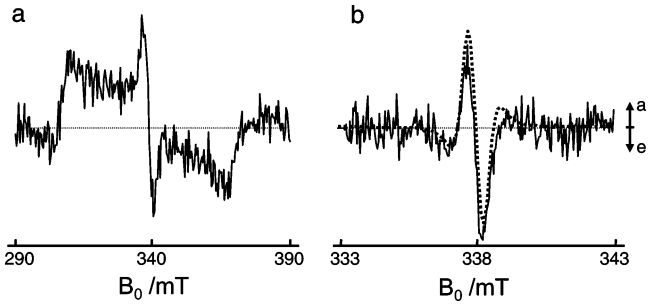

Figure 7. X-band TREPR spectra $\chi''(B_0)$ of photoexcited ZnP−PyrF in THF: (a) at 135 K, 0.8 μs after the laser pulse; (b) at 180 K, 7.0 μs after the laser pulse. The superimposed dotted line is the line shape simulation as described in the text.

complex (≈12 Å),[19] suggesting the formation of a loosely bound RP, which is allowed to occur in the liquid phase, but not in frozen matrices. With further temperature increase the RP signal escapes detection. To summarize, the long-lived RP is consistent with the relatively long separation by R_{cc}.

The energetics associated with the photoexcited ZnP−PyrF in frozen and liquid toluene solutions is summarized in Figure 6. In the case of frozen toluene (Figure 6a), the dominant route to generate ZnP−^{3*}PyrF is via the singlet−singlet EnT, $^{S}k_{EnT}$. The RP energy level, in terms of results discussed earlier, should be lower or isoenergetic with that of ^{3*}ZnP−PyrF. Nevertheless, the yield of RP formation is very small. In the liquid phase (Figure 6b) the ET process is more efficient due to the larger driving forces, thus placing the energy level of the RP below those of ^{3*}ZnP−PyrF and ZnP−^{3*}PyrF. The temporal behavior of the RP polarization pattern (cf. Figure 3b and Figure 4) confirms that both ET routes, $^{S}k_{ET}$ and $^{T}k_{ET}$, are active.

THF. Except for the line intensities, which are weaker in THF, the spectra recorded in frozen THF (Figure 7a) exhibit the same features as those found in frozen toluene (Figure 3a). Similar to toluene, we observe both components, ^{3*}ZnP−PyrF and ZnP−^{3*}PyrF, but with a poor S/N ratio. In addition, the ratio (ZnP−^{3*}PyrF)/(^{3*}ZnP−PyrF) in THF is smaller than that observed in toluene. No RP spectra were detected in the entire temperature range of frozen THF.

At 180 K, in the liquid phase of THF, no spectra of ^{3*}ZnP−PyrF or ZnP−^{3*}PyrF were detected. Under these conditions, a long-lived spectrum at $g \sim 2$ evolved, exhibiting an **e**, **a**, **e**, **a** polarization pattern (Figure 7b). Also, the spectral behavior under these conditions is similar to that in liquid toluene with the exception that no signal phase inversion could be detected

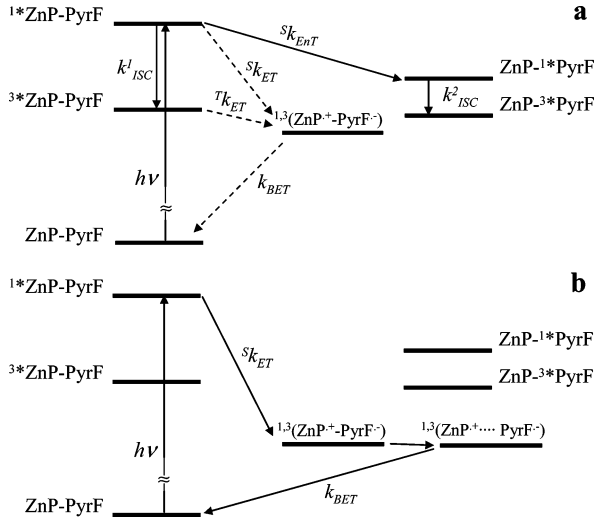

Figure 8. Energy level diagram (unscaled) of ZnP−PyrF in (a) frozen and (b) liquid THF. The energy level positions are the same as in Figure 6.

(Figure 4b). The spectrum shown in Figure 7b was simulated as a TRP formed by S−T_0 mixing mechanism (singlet precursor) with ZFS parameters $D = -0.7$ mT and $E = 0.1$ mT (uncertainty is ±5% and ±20%, respectively), i.e., the same as those obtained in liquid toluene at 200 K (Figure 3b). A singlet precursor of the RP is in line with the fact that the triplet constituents ^{3*}ZnP−PyrF and ZnP−^{3*}PyrF were not detected. As in the case of liquid toluene, this D value corresponds to a distance (R_{cc}) of 15.7 Å, calculated using the dipole−dipole approximation. However, the conspicuous difference between the TRP spectra, in liquid toluene and liquid THF, is in their kinetics (Figure 4). TRP in THF arises much slower than in toluene and lives much longer, without change in the polarization pattern. The kinetic trace of the RP was fit using eq 1 with $A_3 = 0$. The obtained parameters are presented in Table 1. To summarize, the experimental observations show that the singlet−singlet EnT in the frozen THF matrix ($^{S}k_{EnT}$ in Figure 8a) is less effective than in frozen toluene. However, the relatively weak ^{3*}ZnP−PyrF spectrum points to the possibility of an additional transfer route which effectively competes with k^{1}_{ISC} in the ZnP moiety. Despite the fact that no RP signals were detected, the only reasonable option for such a competitive process is ET from ^{1*}ZnP−PyrF ($^{S}k_{ET}$) and/or ^{3*}ZnP−PyrF ($^{T}k_{ET}$), which would result in short-lived RPs with lifetimes below TREPR detection capability. In liquid THF (Figure 8b) singlet-initiated ET becomes dominant over all other possible routes. The subtle, but significant differences in the rate constants of the various processes in the two solvents, toluene and THF, become perceptible when comparing Figures 6 and 8.

As in liquid toluene, the experimentally estimated $R_{cc} = 15.7$ Å, corresponding to the loosely bound RP, $^{1,3}(ZnP^{\bullet+}\cdots PyrF^{\bullet-})$.

Liquid Crystalline Matrices. ***E-7.*** In the crystalline phase of E-7 both triplets, ^{3*}ZnP−PyrF and ZnP−^{3*}PyrF, were observed in our TREPR experiments. Also here, the contribution of the triplet spectrum of the fullerene part is stronger, as compared to the control experiment (Figure 9).

No RP signals were detected in the crystalline phase of E-7. In the soft crystalline and nematic phases only the L||B spectra could be observed. At 240 K (Figure 10a) the spectrum of ^{3*}ZnP−PyrF could be detected only at early times (∼0.4 μs after the laser pulse). The spectrum of ZnP−^{3*}PyrF, however, is easily observed, and from ∼2.0 μs onward it is accompanied

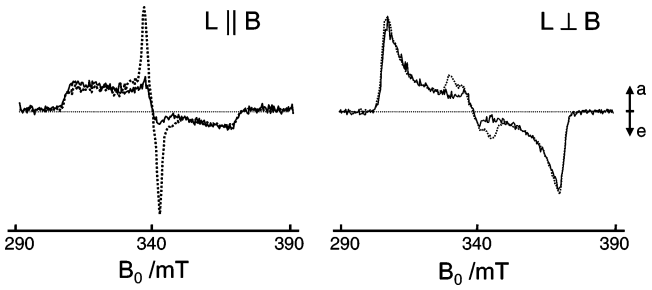

Figure 9. X-band TREPR spectra $\chi''(B_0)$ of ZnP−PyrF (dotted) and ZnP:C_{60} mixture (solid), taken in E-7 at 130 K, 0.8 μs after the laser pulse.

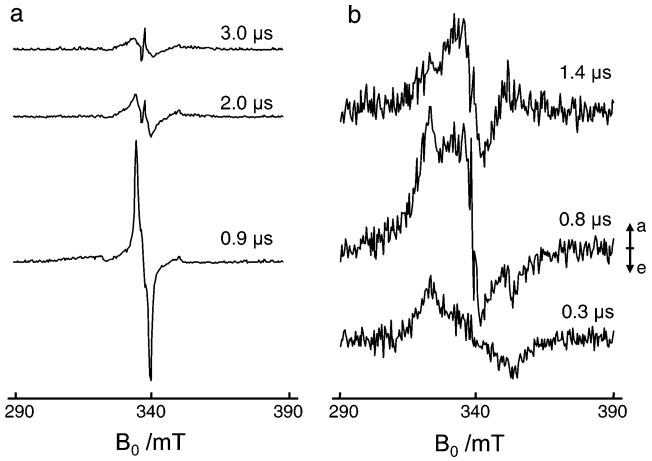

Figure 10. X-band TREPR spectra $\chi''(B_0)$ of photoexcited ZnP−PyrF in E-7 in L||B configuration: (a) at 240 K and (b) at 280 K, at different times after the laser pulse.

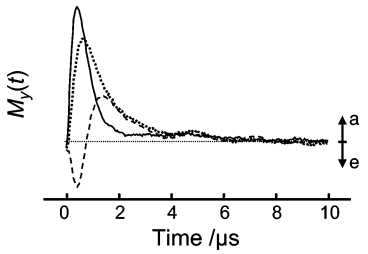

Figure 11. Kinetic profiles of ZnP−PyrF complex in E-7 at 280 K: ^{3*}ZnP−PyrF (solid); ZnP−^{3*}PyrF (dotted); RP, ZnP$^{\bullet+}$−PyrF$^{\bullet-}$ (dashed).

by the sharp spectrum attributed to the RP, featuring an **e**, **a** pattern (Figure 10a). As in the case of frozen toluene, the RP signal is present also at early times, showing an **a**, **e** pattern, but is almost masked by the strong ZnP−^{3*}PyrF spectrum. These observations indicate photochemical routes that are similar to those in frozen toluene.

The spectra taken in the nematic phase of E-7 (260−280 K) exhibit a low S/N ratio and are a superposition of the spectra attributed to all species, i.e., triplets and the RP (Figure 10b). The RP signal at $g \sim 2$ exhibits a change in the polarization pattern from **a**, **e** at 0.8 μs after the laser pulse to **e**, **a** at ∼1.4 μs.

The kinetic traces corresponding to ^{3*}ZnP−PyrF, ZnP−^{3*}PyrF and ZnP$^{\bullet+}$−PyrF$^{\bullet-}$, taken at 280 K, are shown in Figure 11. The rise time of ZnP−^{3*}PyrF signal is slower than that of ^{3*}ZnP−PyrF. It suggests a slow buildup of ZnP−^{3*}PyrF via singlet−singlet EnT ($^{S}k_{EnT}$ in Figure 12). This EnT generates ZnP−^{1*}PyrF followed by a slow generation of the ZnP−^{3*}PyrF signal. A slow buildup of the triplet manifold was also found in pristine $^{3*}C_{60}$.[20−26] Furthermore, the RP kinetic profile demonstrates that its phase inversion coincides with the disappearance of ^{3*}ZnP−PyrF, thus confirming that the origin of the RP (**e,a** pattern) is ^{3*}ZnP−PyrF. The kinetic trace of the RP at 280 K was fit with eq 1 (see Table 1). At temperatures above 280 K, all signals are vanishingly small. To summarize, in the crystalline phase of E-7, efficient singlet−singlet EnT ($^{S}k_{EnT}$), ^{1*}ZnP−PyrF → ZnP−^{1*}PyrF, is the main transfer route. In the soft crystalline phase, singlet−singlet EnT is accompanied by singlet- and triplet-initiated ET ($^{1}k_{ET}$ and $^{3}k_{ET}$). At low temperatures of the nematic phase, the slow rise time of ZnP−^{3*}PyrF reflects the slower rate of singlet−singlet EnT. As to the RP spectrum, the temporal change in the polarization pattern indicates that both ET routes, i.e., singlet- and triplet-initiated, are active. At high temperatures of the nematic phase and in the isotropic phase, all signals escape detection, probably due to the fast ET and BET processes. The energetics of the system in the different phases of E-7 is presented in Figure 12. Again, it is interesting to compare Figure 12 with Figures 6 and 8 to visualize the subtle differences of the transfer processes in the different solvent matrices.

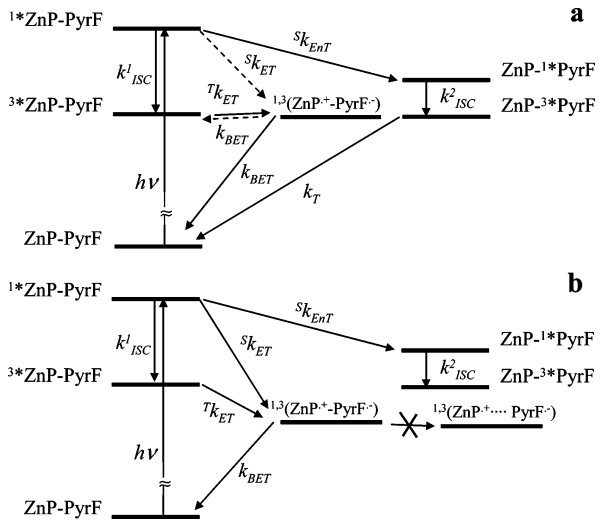

Figure 12. Energy level diagram (unscaled) of ZnP−PyrF in E-7: (a) soft glass; (b) nematic phase. The energy level positions are the same as in Figure 6.

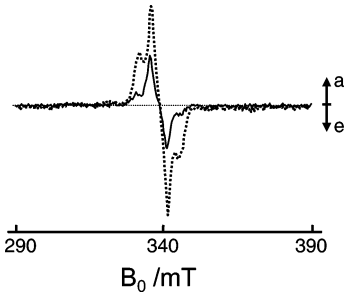

Figure 13. X-band TREPR spectra $\chi''(B_0)$ of photoexcited ZnP−PyrF in ZLI-4389 at 170 K, taken at 0.8 μs after the laser pulse: solid, L||B; dotted, L⊥B.

No long-lived RP was detected in E-7 at any temperature. It is noteworthy that the lifetime of the RP (Table 1), as observed in the fluid phase of E-7, is much shorter than the lifetime in isotropic liquids. We attribute this behavior to the allowed ^{1,3}(ZnP$^{\bullet+}$−PyrF$^{\bullet-}$) → ^{1,3}(ZnP$^{\bullet+}$···PyrF$^{\bullet-}$) partial dissociation process in toluene and THF, while in E-7 this process is unlikely.

ZLI-4389. In the crystalline phase of the more polar LC, ZLI-4389, only the ZnP−^{3*}PyrF spectrum could be observed over the temperature range 130−250 K (Figure 13).

The fact that the ^{3*}ZnP−PyrF spectrum was not detected suggests that both ^{1*}ZnP−PyrF and/or ^{3*}ZnP−PyrF were

completely depleted by fast relaxation or transfer processes. No RP spectra were detected over this temperature range. The line shape of the ZnP−^{3*}PyrF spectrum is similar to that of the monomer, ^{3*}PyrF. Therefore, it is reasonable to assume that ZnP−^{3*}PyrF was formed by ISC from ZnP−^{1*}PyrF, indicating an efficient singlet−singlet EnT process. At higher temperatures, in the nematic and isotropic phases, all signals are vanishingly small, probably due to fast ET. Similar to toluene vs THF, the different results obtained using E-7 and ZLI-4389 can be attributed to the different polarity of these two LCs. It is noteworthy, that in the covalently linked parachute-shaped ZnP−C_{60} dyad studied recently[26] and in other covalently linked D−A systems[36] the experimental results were found to be independent of the LC polarity. This discrepancy can be resolved by considering the additional degree of freedom of the complex studied in the present work, which affects the reorganization energy, λ_s. The parameters required for calculating λ_s at the corresponding temperatures in the relevant LCs, are not available. However, the importance of the polarity effect in complex **2** enables us to analyze the results for the isotropic solvents and to apply this analysis also to the anisotropic LC matrices.

As shown in Table 1, the temporal behavior of the RPs strongly depends on the solvents. In terms of Marcus theory, the rate constant for electron transfer, k_{ET}, is given by[49]

$$k_{ET} = \frac{2\pi}{\hbar}|V|^2(\mathrm{FC}) \tag{2}$$

where V is the electronic coupling matrix element and FC is the averaged nuclear Franck−Condon factor. In the classical limit for a nonadiabatic process, the ET rate is expressed by eq 3,

$$k_{ET} = A|V|^2 e^{-E_a/kT} = \frac{2\pi|V|^2}{\hbar\sqrt{4\pi\lambda_s kT}} \exp\left[-\frac{(\Delta G_{CS}{}^0 + \lambda_s)^2}{4\lambda_s kT}\right] \tag{3}$$

where $\Delta G_{CS}°$ is the free-energy of charge separation and λ_s is the solvent reorganization energy. For toluene and THF, λ_s was calculated according to eq 4[50]

$$\lambda_s = \frac{e^2}{2}\left(\frac{1}{r_A} + \frac{1}{r_D} - \frac{2}{R_{cc}}\right)\left(\frac{1}{n_D{}^2} - \frac{1}{\epsilon_s}\right) \tag{4}$$

where r_D and r_A are the effective radii of the donor and the acceptor, R_{cc} is the center-to-center D−A distance, e is the electron charge, and ϵ_s and n_D are the static dielectric constant and the refractive index of the solvent. The following parameters were used in the calculations: $r_D = 7.5$ Å (for ZnP, as was extracted from the molecular modeling), $r_A = 4$ Å (for PyrF), and $R_{cc} = 12$ Å. As to n_D and ϵ_s, they were calculated to be 1.548 and 2.63 for toluene at 200 K and 1.405 and 10.89 for THF at 180 K, respectively.[51] The significant difference obtained for the values of the solvent reorganization energy at similar temperatures, namely, 0.06 eV for toluene at 200 K and 0.62 eV for THF at 180 K, might account for the difference between the ET and BET rates in these solvents. Furthermore, the dependence of V on the molecular structure and medium properties is most noticeable when the coupling between the donor and acceptor is weak, as it is in our coordinative linkage case. It is noteworthy that, unlike for the ZnP−PyrF complex **2**, no significant difference in k_{ET} or k_{BET} was noticed for the covalently linked D−s−A systems studied previously by TREPR in various solvents.[26,36] It is reasonable to assume that due to their covalent linkage, the latter systems are less flexible, thus leaving the electronic coupling in different solvents unchanged. In our case, the much higher reorganization energy of THF as compared to toluene, results in a decrease of the forward and backward ET rates.[50] We rule out the effects of solvent viscosity since the calculated viscosities at the corresponding temperatures are similar, namely 4.7 cP for toluene at 200 K and 5.0 cP for THF at 180 K.[51] To summarize, the changes in the activation energy of the process together with changes in V and λ_s (eq 3), can easily account for the differences in the ET and BET rate constants in toluene and THF (see Table 1).

Conclusions

The experimental results presented in this work confirm the hypothesis[18,19] concerning the existence of an equilibrium between association and dissociation of the coordinatively linked "metal-pyridine" ZnP−C_{60} complex. This complexation facilitates, after photoexcitation, rapid intramolecular EnT and/or ET to produce a triplet radical pair, which occurs in polar as well as in nonpolar solvents. When partial dissociation of the complex constituents is allowed (in liquid phases of isotropic solvents), the partial or complete separation of the components slows down the BET process, thus generating a long-lived radical ion pair. In a frozen matrix, where this splitting is inhibited, EnT is the dominant process. The ordered LC matrix prevents the separation of the complex constituents, thus hindering the creation of long-lived radical pairs even in fluid phases.

It is noteworthy that in covalently linked D−s−A systems the utilization of LCs generally results in ET rates that are reduced by several orders of magnitude, as compared to those in isotropic solvents.[21] This reduction of ET rates is due to the nematic potential associated with the alignment of the LC molecules, which restricts the isotropic molecular reorientation found in conventional solvents. Such an effect was not found for the reported coordinatively linked D−s−A system. Moreover, in contrast to the present case, the results obtained in different LCs for covalently linked D−s−A systems were found to be independent of LC's polarity.[26,36] Thus, the noncovalent ZnP−PyrF system **2** enables direct exploitation of the matrix polarity to control ET and BET processes in both isotropic and anisotropic matrices.

Acknowledgment. The Farkas Center is supported by the Bundesministerium für Bildung und Forschung and by Minerva Gesellschaft für die Forschung GmbH. This work was supported by the Israel Science Foundation and the Ministry of Science (H.L.), and by the DFG (H.L., K.M. and A.S. in the framework of the SFB 498 program). The work at NYU was supported by grants from the U. S. National Science Foundation. Discussions with Mr. E. Stavitski (Jerusalem) are highly appreciated.

References and Notes

(1) Gust, D.; Moore, T. A.; Moore, A. L. *Acc. Chem. Res.* **2001**, *34*, 40.

(2) Cravino, A.; Sariciftci, N. S. *J. Mater. Chem.* **2002**, *12*, 1931.

(3) Yamada, H.; Imahory, H.; Nishimura, Y.; Yamazaki, I.; Ahn, T. K.; Kim, S. K.; Kim, D.; Fukuzumi, S. *J. Am. Chem. Soc.* **2003**, *125*, 9129.

(4) Guldi, D. M. *Chem. Commun.* **2000**, 321.

(5) Bracher, P. J.; Schuster, D. I. Electron Transfer in Functionalized Fullerenes. In *Fullerenes: From Synthesis to Optoelectronic Applications*; Guldi, D. M.; Martin, N., Eds.; Kluwer Academic Publishers: Dordrecht, The Netherlands, 2002; p 163.

(6) Imahori, H.; Hagiwara, K.; Akiyama, T.; Aoki, M.; Taniguchi, S.; Okada, T.; Shirakawa, M.; Sakata, Y. *Chem. Phys. Lett.* **1996**, *263*, 545.

(7) Ward, M. D. *Chem. Soc. Rev.* **1997**, *26*, 365.

(8) Guldi, D. M.; Luo, C. P.; Prato, M.; Dietel, E.; Hirsch, A. *Chem. Commun.* **2000**, 373.

(9) Guldi, D. M.; Ramey, J.; Martinez-Diaz, M. V.; de la Escosura, A.; Torres, T.; Da Ros, T.; Prato, M. *Chem. Commun.* **2002**, 2774.
(10) Meijer, M. D.; van Klink, G. P. M.; van Koten, G. *Coord. Chem. Rev.* **2002**, *230*, 141.
(11) D'Souza, F.; Deviprasad, G. R.; Rahman, M. S.; Choi, J. P. *Inorg. Chem.* **1999**, *38*, 2157.
(12) Da Ros, T.; Prato, M.; Guldi, D. M.; Ruzzi, M.; Pasimeni, L. *Chem.—Eur. J.* **2001**, *7*, 816.
(13) D'Souza, F.; Deviprasad, G. R.; El-Khouly, M. E.; Fujitsuka, M.; Ito, O. *J. Am. Chem. Soc.* **2001**, *123*, 5277.
(14) D'Souza, F.; Gadde, S.; Zandler, M. E.; Arkady, K.; El-Khouly, M. E.; Fujitsuka, M.; Ito, O. *J. Phys. Chem. A* **2002**, *106*, 12393.
(15) D'Souza, F.; Deviprasad, G. R.; Zandler, M. E.; El-Khouly, M. E.; Fujitsuka, M.; Ito, O. *J. Phys. Chem. B* **2002**, *106*, 4952.
(16) D'Souza, F. *J. Phys. Chem. A* **2002**, *106*, 3243.
(17) D'Souza, F.; Deviprasad, G. R.; Zandler, M. E.; El-Khouly, M. E.; Fujitsuka, M.; Ito, O. *J. Phys. Chem. A* **2003**, *107*, 4801.
(18) Wilson, S. R.; MacMahon, S.; Tat, F. T.; Jarowski, P. D.; Schuster, D. I. *Chem. Commun.* **2003**, 226.
(19) Tat, F. T.; Zhou, Z. G.; MacMahon, S.; Song, F. Y.; Rheingold, A. L.; Echegoyen, L.; Schuster, D. I.; Wilson, S. R. *J. Org. Chem.* **2004**, *69*, 4602.
(20) Levanon, H. *Adv. Photosynth.* **1996**, *3*, 211.
(21) Levanon, H.; Hasharoni, K. *Prog. React. Kinet.* **1995**, *20*, 309.
(22) Hasharoni, K.; Levanon, H. *J. Phys. Chem.* **1995**, *99*, 4875.
(23) Levanon, H.; Galili, T.; Regev, A.; Wiederrecht, G. P.; Svec, W.; Wasielewski, M. R. *J. Am. Chem. Soc.* **1998**, *120*, 6366.
(24) Wiederrecht, G. P.; Svec, W. A.; Wasielewski, M. R.; Galili, T.; Levanon, H. *J. Am. Chem. Soc.* **2000**, *122*, 9715.
(25) Shaakov, S.; Galili, T.; Stavitski, E.; Levanon, H.; Lukas, A.; Wasielewski, M. R. *J. Am. Chem. Soc.* **2003**, *125*, 6563.
(26) Galili, T.; Regev, A.; Levanon, H.; Schuster, D. I.; Guldi, D. M. *J. Phys. Chem. A* **2004**, *108*, 10632.
(27) Berg, A.; Galili, T.; Levanon, H.; Kotlyar, A. B.; Hazani, M. *J. Phys. Chem. A* **1999**, *103*, 8372.
(28) Mobius, K.; Savitsky, A.; Schnegg, A.; Plato, M.; Fuchs, M. *Phys. Chem. Chem. Phys.* **2005**, *7*, 19.
(29) http://www.bandj.com/BJSolvents; Honeywell, B. J. **2004.**
(30) Merck, E. *Merck Ltd. Catalog: Nematic Liquid Crystal Mixtures*; Merck: Whitehouse Station, NJ, 1989.
(31) Gonen, O.; Levanon, H. *J. Chem. Phys.* **1986**, *84*, 4132.
(32) Sun, Y.-P. Photoexcited States and Charge-Transfer Properties of Fullerene Materials. *Fullerenes. Recent advances in the chemistry and physics of fullerenes and related materials*; Reno, Nevada, 1995.
(33) As will be shown below, the existence of the two conformers is confirmed by TREPR results.
(34) Levanon, H.; Bowman, M. K. *Time-domain EPR spectroscopy of energy and electron transfer*; Academic Press Inc.: New York, 1993.
(35) Hasharoni, K.; Levanon, H.; von Gersdorff, J.; Kurreck, H.; Möbius, K. *J. Chem. Phys.* **1993**, *98*, 2916.
(36) Hasharoni, K.; Levanon, H.; Greenfield, S. R.; Gosztola, D. J.; Svec, W. A.; Wasielewski, M. R. *J. Am. Chem. Soc.* **1996**, *118*, 10228.
(37) Berman, A.; Izraeli, E. S.; Levanon, H.; Wang, B.; Sessler, J. L. *J. Am. Chem. Soc.* **1995**, *117*, 8252.
(38) Asano, M.; Kaizu, Y.; Kobayashi, H. *J. Chem. Phys.* **1988**, *89*, 6567.
(39) Berg, A.; Shuali, Z.; Asano-Someda, M.; Levanon, H.; Fuhs, M.; Möbius, K.; Wang, R.; Sessler, J. L. *J. Am. Chem. Soc.* **1999**, *121*, 7433.
(40) Wiederrecht, G. P.; Svec, W. A.; Wasielewski, M. R.; Galili, T.; Levanon, H. *J. Am. Chem. Soc.* **1999**, *121*, 7726.
(41) Fujisawa, J.; Ohba, Y.; Yamauchi, S. *Chem. Phys. Lett.* **1998**, *294*, 248.
(42) Schuster, D. I.; Cheng, P.; Jarowski, P. D.; Guldi, D. M.; Luo, C.; Echegoyen, L.; Pyo, S.; Holzwarth, A. R.; Braslavsky, S. E.; Williams, R. M.; Klihm, G. *J. Am. Chem. Soc.* **2004**, *126*, 7257.
(43) Guldi, D. M.; Maggini, M.; Scorrano, G.; Prato, M. *J. Am. Chem. Soc.* **1997**, *119*, 974.
(44) Armaroli, N.; Diederich, F.; Echegoyen, L.; Habicher, T.; Flamigni, L.; Marconi, G.; Nierengarten, J. F. *New J. Chem.* **1999**, *23*, 77.
(45) Prato, M.; Maggini, M. *Acc. Chem. Res.* **1998**, *31*, 519.
(46) Guldi, D. M.; Prato, M. *Acc. Chem. Res.* **2000**, *33*, 695.
(47) Felton, R. H. **1978**.
(48) Dubois, D.; Jones, M. T.; Kadish, K. M. *J. Am. Chem. Soc.* **1992**, *114*, 6446.
(49) Marcus, R. A. *Annu. Rev. Phys. Chem.* **1964**, *15*, 155.
(50) Kaplan, R.; Napper, A. M.; Waldeck, D. H.; Zimmt, M. B. *J. Phys. Chem. A* **2002**, *106*, 1917.
(51) Marcus, Y. *The Properties of Solvents*; John Wiley & Sons: Chichester, U.K., 1998; Vol. 4.